



A Novel Tri-bandpass Filter Side-coupled Square Ring Based

José Garibaldi Duarte Júnior¹ , Valdemir Praxedes da Silva Neto² 

¹ Postgraduate Program in Electrical and Computer Engineering – PPGEEC/UFRN, Natal, RN, Brazil,
garibaldijrn@gmail.com

² Communication Engineering Department – DCO/UFRN, Natal, RN, vpraxedes.neto@gmail.com

Abstract— This work presents the design of a tri-bandpass filter based on the side-coupled square ring structure. The modeling is conceived from the classic approach of coupled transmission lines. The geometry consists of a square structure of electrical length equal to twice the wavelength of the main operating frequency, and the laterally coupled lines through which the power supply occurs. Expressions for the admittance and transformation matrix were obtained based on the impedances and admittances that model the geometry. Analyzis were performed from EM simulations. A prototype was built to validate the modeling and adjusted for operation at 0.78, 1.5 and 2.30 GHz. All results are discussed and commented, and the comparisons between simulated and measured results are coherent and in agreement, thus proving the effectiveness of the applied method.

Index Terms—Tri-band Bandpass Filter, Side-coupled Square Ring, Transmission Line.

I. INTRODUCTION

Research involving radio frequency filters follows a growing constant as well as the development of microwave-based communication systems. Microwave circuit research and design focused on signal frequency filtering is a field of research that has continued to advance over the past few decades and gain adepts. Due to the constant advances in telecommunication systems, the demand for low cost, compact filters and increasingly specific frequency response is a tendency to be met.

Over the past few years, researchers have developed microwave planar filters based primarily on transmission line modeling [1] - [4] and, with dual-mode or multi-mode resonator behavior, syntheses have been made to from even and odd excitation circuit analysis to obtain expressions that contribute to resonator modeling and filter response [5] - [12]. The methodology based on mode analysis is also applicable in the development of bandstop structures [21]. Techniques such as the use of Substrate Integrated Waveguide (SIW) structures to improve filter performance [22] - [23] are also valid. Much of the research involving microwave filters commonly seeks the development of performance bandpass planar circuits with one or more transmission bands and high frequency selectivity, as well as high attenuation rates in reject bands. In [13], a bandpass filter is developed in microstrip using coupled lines, a common practice. A transmission line modeling is applied to obtain the coupling matrix of the circuit, and the resonance frequency is investigated as a function of the variation of the resonator key parameters. With a similar methodology, in [14] a compact dual-wideband bandpass filter is proposed.

The established resonator is based on the coupling of a pair of shorted grounded conductor strips parallel to the main transmission line. Using a coupling feed, in [6] a hexagonal patch is proposed along with the use of hollow fractal elements. A bandpass response is obtained from an even and odd mode analysis for the resonator. Based on the fully modeled side-coupled ring resonator proposed in [3] and from the use of stub-loads, in [2] a bandpass filter with a high selectivity index and an increase of zero transmission frequencies is developed when compared to [2], this behavior is due to the use of coupling between lines and stub-loads.

In this work, a tri-bandpass filter (TBF) is proposed. The resonator structure is inspired by the side-coupled ring geometry presented in [2] due to its bandwidth, well-defined zero transmission frequencies and its fully delimited synthesis. In order to introduce new operating bands, important changes are attributed to the resonator geometry. An analysis of the proposed resonator is performed with the objective of modeling the TBF and obtaining expressions that govern its frequency response as a function of the main resonator parameters. Simulations performed in transmission line and microwave circuit analysis software are presented and a prototype filter is constructed and subjected to experimental measurement process. Section II of this paper deals with the mathematical modeling of the resonator. Simulations and analyzes are presented in section III. In item IV, the prototype design is developed and the simulation and measurement results are analyzed and compared. Finally, a conclusion is presented in item V.

II. RESONATOR MODEL

Fig. 1(a) and (b) show the planar structure resonator (TBF) proposed in this work and its transmission line modeling, respectively. The geometry of the resonator resembles the side-coupled square loop ring present in [2], but its perimeter length totals about 2λ of the main resonant frequency. In [2] and [3], the use of the square-ring resonator with 1λ provides a frequency performance with a single operating band. In this model, a geometry of total length 2λ is proposed, which allows obtaining two additional lateral bands in the frequency response compared to [3]. As can be seen, the ports are set at an angle of $\pi/4$ rad. The resonator geometry can be subdivided into three parts: two pairs of laterally coupled transmission lines of impedances Z_{oe} , Z_{oo} and electrical length $3\lambda/4$, and a characteristic half-wavelength impedance centerline Z_L and θ_{el} of the TBF center frequency. Coupled pairs of lines are interconnected with each other, while impedance Z_L makes the connection between them at the opposite vertex of the geometry. Thus, the length L on either side of the square-loop ring is approximately half wavelength of the central resonant frequency of the TBF.

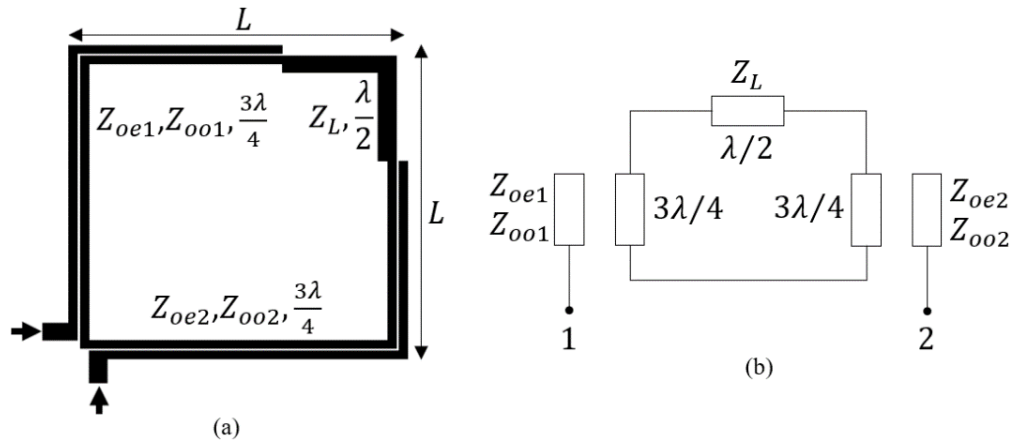


Fig. 1. Tri-band Bandpass Filter. (a) TBF Resonator geometry. (b) Equivalent circuit modeled on transmission line.

A. Three-port Coupled-lines Modeling

The modeling of coupled line pairs present in the proposed resonator follows the methodology presented in [15]. A classic approach to coupled lines is developed and focuses on networks based on lines with an N number of ports. This paper presents an analysis of three-port coupled line networks, one of which is open circuit terminations. This approach is then used as a starting point for the resonator modeling proposed here. Fig. 2 shows the 3-port coupled line network and its equivalent circuit based on the analysis in [15].

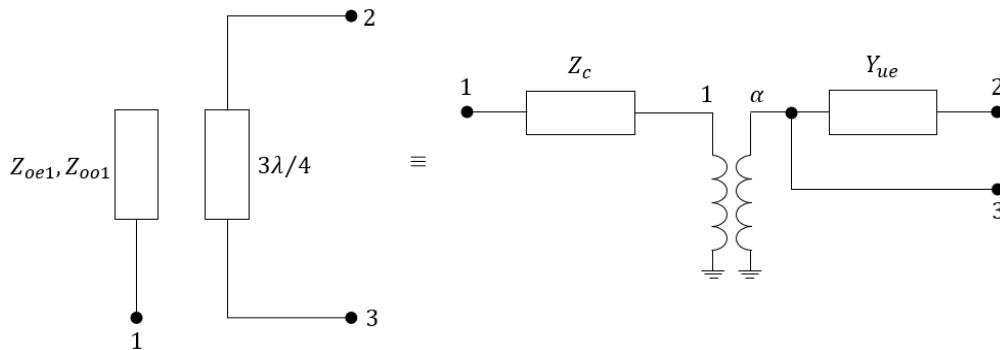


Fig. 2. Network of coupled lines with three ports and their corresponding circuit based on [15].

The impedance Z_c models the capacitive coupling and the losses present in the region between the conductive tapes. The coupling is modeled through the ideal transformer ratio transformer α , through which the electrical signal flows without physical contact between the coupled lines. Lastly, admittance Y_{ue} describes the admittance of network input. Based on the analyzes made in [15], [16] and [17], all these parameters can be written as a function of odd and even mode impedances (Z_{oe} and Z_{oo}):

$$s = j \tan \theta \quad (1)$$

$$Y_c = s Y_{11} \quad (2)$$

$$\alpha = \frac{Y_{11}}{Y_{12}} \quad (3)$$

$$Y_{ue} = Y_{11} - \frac{Y_{12}^2}{Y_{11}} \quad (4)$$

Where the parameter s is being the so-called Richards variable [17]. According to [16], admittances Y_{11} and Y_{12} can be respectively written as follows in (5) and (6)..

$$Y_{11} = \frac{(Y_{oo} + Y_{oe})}{2} \tag{5}$$

$$Y_{12} = \frac{(Y_{oo} - Y_{oe})}{2} \tag{6}$$

where $Y_{oo} = 1/Z_{oo}$ and $Y_{oe} = 1/Z_{oe}$. Finally, the admittance Y_{ue} of Fig. 2 can be written according to transformation matrix A :

$$A = \frac{1}{\sqrt{1-s^2}} \begin{bmatrix} 1 & s/Y_{ue} \\ sY_{ue} & 1 \end{bmatrix} \tag{7}$$

B. Equivalent Circuit Assembly

From the analysis of the equivalent circuit for the three-port coupled line network presented in the previous subsection and considering A_L (8) as the transformation matrix of a characteristic impedance line Z_L and electrical length θ , it is possible to write the admittance matrix Y_s shown in Fig. 3.

$$A_L = \begin{bmatrix} \cos \theta & jZ_L \sin \theta \\ \frac{j \sin \theta}{Z_L} & \cos \theta \end{bmatrix} \tag{8}$$

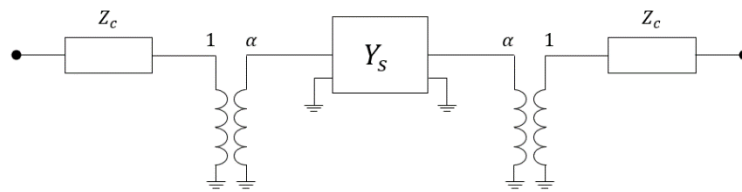


Fig. 3. Equivalent circuit composition of coupled lines and admittance matrix Y_s .

Through some algebraic operations and manipulations, it is possible to write the transformation matrix A_s and admittance Y_s that help describe the circuit that shapes the geometry as follows:

$$A_s = \frac{1}{1-s^2} \begin{bmatrix} A_{11} & A_{12} \\ A_{21} & A_{22} \end{bmatrix} \tag{9}$$

$$A_{11} = \frac{Y_{ue} Z_L \cos \theta_L + js \sin \theta_L + js Y_{ue}^2 Z_L^2 \sin \theta_L + s^2 Y_{ue} Z_L \cos \theta_L}{Y_{ue} Z_L} \tag{10}$$

$$A_{12} = \frac{2s Y_{ue} Z_L \cos \theta_L + js^2 \sin \theta_L + j Y_{ue}^2 Z_L^2 \sin \theta_L}{Y_{ue}^2 Z_L} \tag{11}$$

$$A_{21} = \frac{2s Y_{ue} Z_L \cos \theta_L + j \sin \theta_L + js^2 Y_{ue}^2 Z_L^2 \sin \theta_L}{Z_L} \tag{12}$$

$$A_{22} = \frac{Y_{ue} Z_L \cos \theta_L + js \sin \theta_L + js Y_{ue}^2 Z_L^2 \sin \theta_L + s^2 Y_{ue} Z_L \cos \theta_L}{Y_{ue} Z_L} \tag{13}$$

$$Y_s = \begin{bmatrix} Y_{s11} & Y_{s12} \\ Y_{s12} & Y_{s11} \end{bmatrix} \quad (14)$$

$$Y_{s11} = \frac{s^2 Y_{ue}^2 Z_L \cos \theta_L + j s Y_{ue} \sin \theta_L + j s Y_{ue}^3 Z_L^2 \sin \theta_L + Y_{ue}^2 Z_L \cos \theta_L}{2 s Y_{ue} Z_L \cos \theta_L + j s^2 \sin \theta_L + j Y_{ue}^2 Z_L^2 \sin \theta_L} \quad (15)$$

$$Y_{s12} = \frac{Y_{ue}^2 Z_L (1 - s^2)}{2 s Y_{ue} Z_L \cos \theta_L + j s^2 \sin \theta_L + j Y_{ue}^2 Z_L^2 \sin \theta_L} \quad (16)$$

III. ANALYSIS AND SIMULATIONS

Based on the circuit of Fig. 1(b), which provides an equivalence to the resonator geometry, simulations were performed in Advanced Design System (ADS). Taking into account the modeling presented in the previous section, the frequency response of the 1.00 GHz principle resonance frequency f_R circuit was analyzed, as shown in Fig. 4. The impedance parameters employed were: $Z_{oe} = 94 \Omega$, $Z_{oo} = 49 \Omega$ and $Z_L = 50 \Omega$. Electrical lengths were determined according to a study in section II.

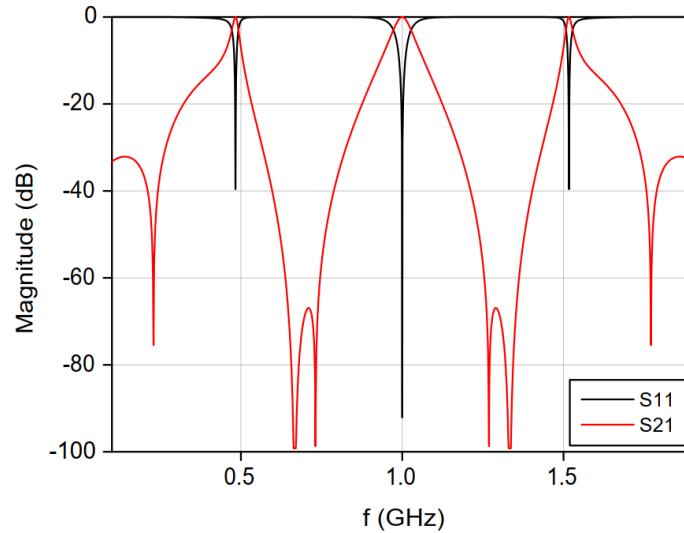


Fig. 4. Frequency response to equivalent circuit considering f_R equal to 1.00 GHz.

As can be seen, the response has a f_R main resonance frequency of 1.00 GHz and two symmetric resonances: lower transmission band (LTB) at 0.483 GHz, and upper transmission band (UTB) at 1.517 GHz. The bandwidth at -3 dB at 1 GHz equal to 54 MHz and at symmetrical transmission bands 20 MHz. The graph of Fig. 5 showing the phase variation of the spreading parameters S11 and S21 as a function of frequency contributes to the verification of the symmetries between LTB and UTB of the filter response.

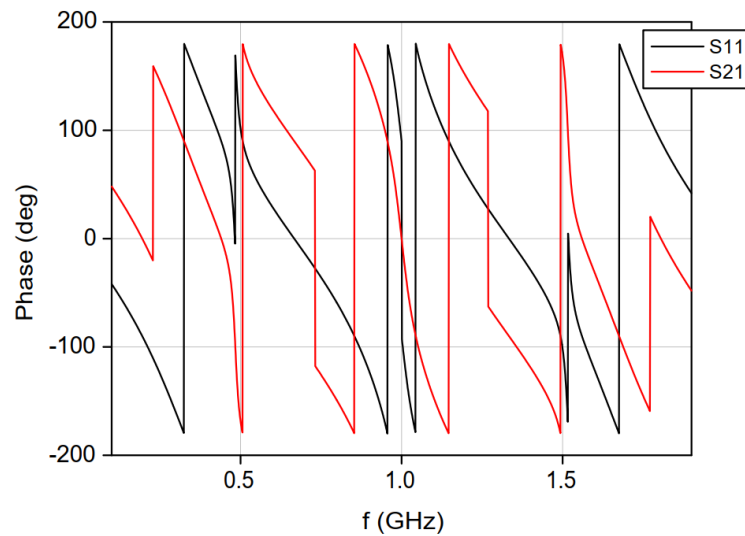


Fig. 5. Frequency response (phase) to equivalent circuit considering f_R equal to 1.00 GHz.

It is also important to note the six symmetrical zero transmission frequencies, which contribute to TBF selectivity. Based on this, two parameters are defined that will facilitate the following analyzes: r and t_z . Parameter r defines the relationship between LTB's first resonant frequency f_1 and the main frequency f_R , where $r = f_1/f_R$. As previously stated, the second resonance f_2 is symmetrical with respect to resonance f_1 and f_R . The parameter t_z represents the relationship between the zero transmission frequency f_{tz} closest to the main transmission band and f_R , so $t_z = f_{tz}/f_R$.

From the established parameters r and t_z , the analysis of these and the bandwidth BW of the main transmission band was performed at -3 dB as a function of the impedances that constitute the equivalent circuit, and consequently, of the resonator geometry in order to have a notion of the influence of each of the impedances on the filter response. According to Fig. 6, which brings the analysis to the previously established parameters, it is possible to make some conclusions. With respect to r , Fig. 6(a), the increase in impedance Z_L provides an approximation of LTB and UTB towards f_R , but for Z_{oo} increase the effect is opposite. The graph in Fig. 6(b) stresses the behavior of parameter t_z as a function of the variation of Z_L and Z_{oo} , presenting a response similar to parameter r . With respect to the BW bandwidth of the main transmission band present in Fig. 6(c), the Z_{oo} increase causes a sharp drop in BW, but with respect to Z_L malfunction, the decrease in BW was much less noticeable. Also, in Fig. 7 it is possible to establish the relationship between r and Z_L for different levels of Z_{oo} impedance. The four curves present similar behavior, presenting a tendency of equilibrium of r for high values of Z_L . It is important to analyze that for each value of Z_{oo} , different levels of constancy of r are observed.

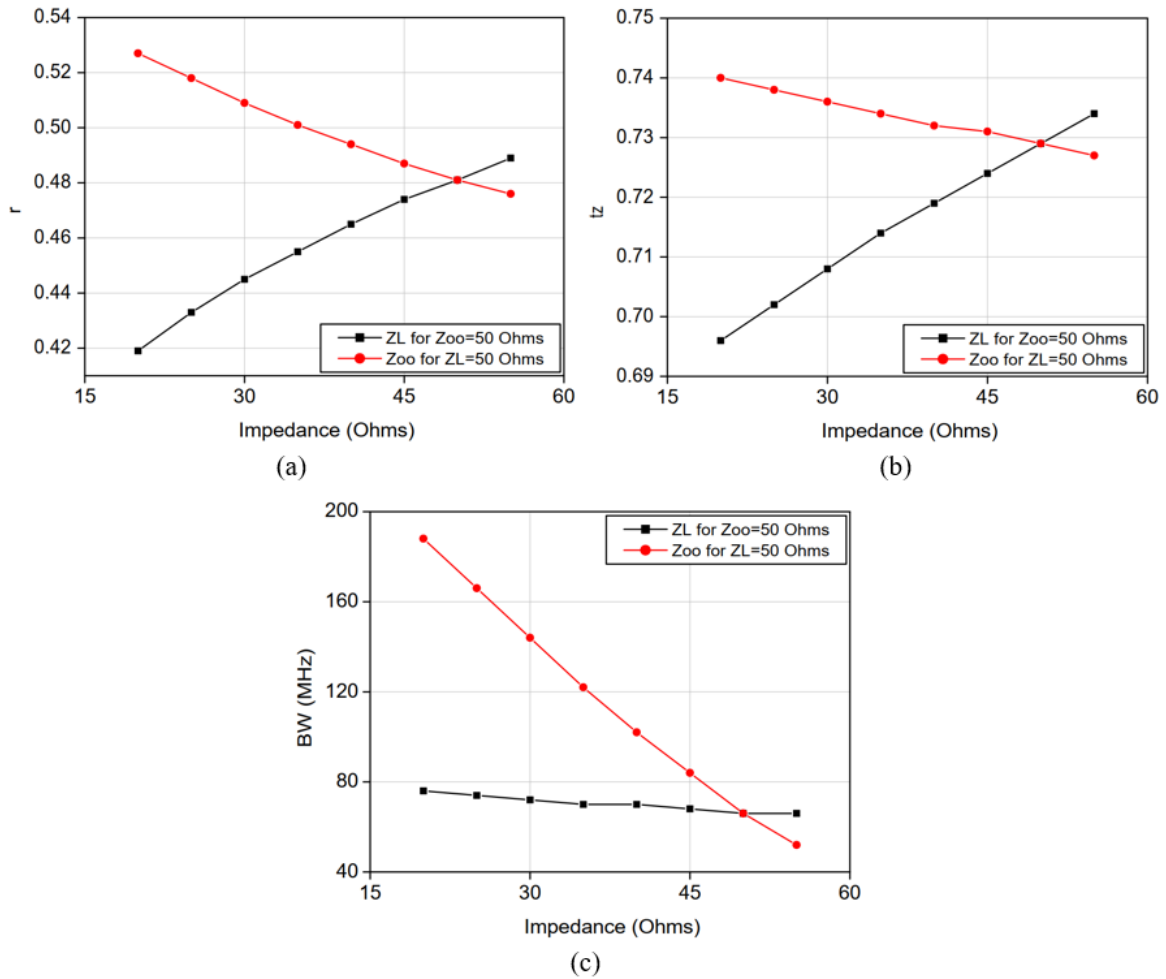


Fig. 6. Equivalent circuit analysis for f_R equal 1.00 GHz and $Z_{oe} = 100 \Omega$. (a) r in function of Z_{oo} e Z_L . (b) tz in function of Z_{oo} and Z_L . (c) BW in function of Z_{oo} and Z_L .

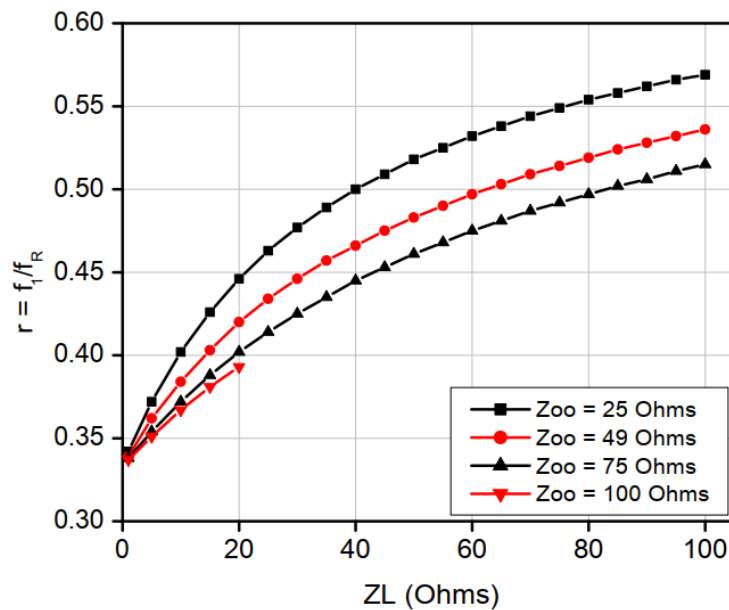


Fig. 7. Analysis of the response of r as a function of Z_L variation for different Z_{oo} values.

IV. TBF FILTER DESIGN, RESULTS AND DISCUSSIONS

From the equivalent circuit modeling and the analyzes performed, a TBF model was implemented in EM simulation software. A geometry with f_R frequency response of 1.50 GHz was proposed, together with LTB and UTB centered at 0.78 and 2.30 GHz, respectively. The model with its respective dimensions is shown in Fig. 8(a). A prototype was built from a RO3006 dielectric plate with a relative permittivity of 6.15, loss tangent of 0.0024 and thickness h of 1.52 mm, as shown in Fig. 8(b), for measurements by means of a network analyzer and obtaining experimental results.

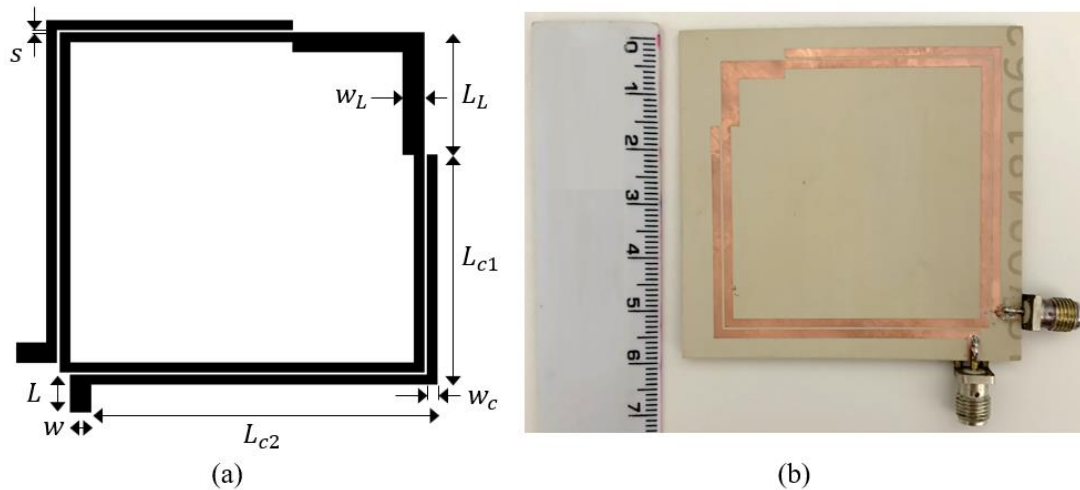


Fig. 8. (a) Tri-bandpass Filter model with $f_R = 1.50$ GHz (dimensions in mm: $s = 0.4$, $w_L = 3.24$, $w_c = 1.58$, $w = 2.24$, $L_L = 11.64$, $L_{c1} = 39$, $L_{c2} = 46.82$, $L = 5.58$). (b) Built prototype.

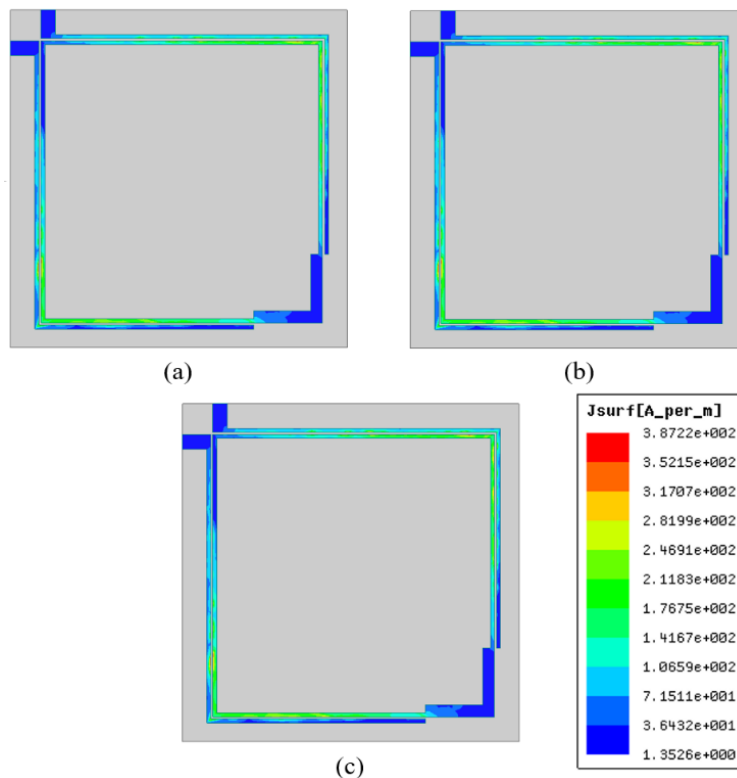


Fig. 9. Surface current density obtained via EM simulation for (a) 0.78 GHz, (b) 1.50 GHz, (c) 2.30 GHz.

The Fig. 9 presents the EM simulation result for the TBF model with respect to surface current density for previously established resonant frequencies. As can be seen, the densities remain almost constant and stable for the different frequencies, presenting only sensitive alterations. The highest A/m levels are concentrated in the central parts of the coupled lines, with the centerline and supply lines having the lowest levels.

The comparison regarding the reflection and transmission parameters of the results obtained by EM simulation and measurement of the built prototype is shown in Fig. 10, showing a good agreement between the curves.

The Table I presents the summary and comparison between the results obtained via EM simulation and experimental measurement of the built prototype. As can be observed, the established and observed simulated resonant frequencies were met with the prototype implementation. Four zero transmission frequencies are observed along the analyzed spectrum, being close to 0.30, 0.96, 1.91 and 2.41 GHz, which contributes to the filter selectivity level.

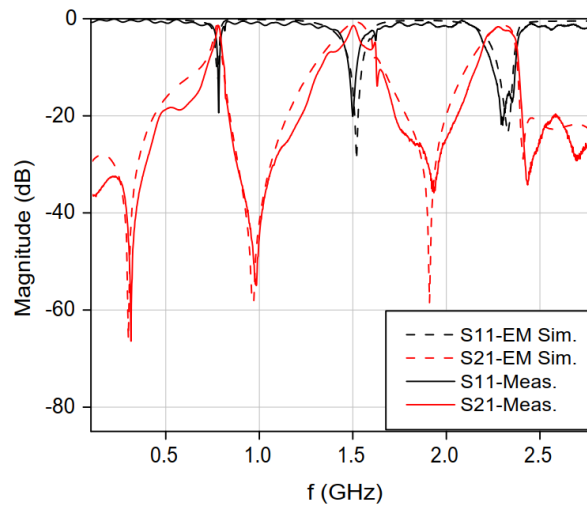


Fig. 10. Comparison of frequency response of results obtained by EM simulation and experimental measurement.

TABLE I. SUMMARY OF RESULTS OBTAINED VIA EM SIMULATION AND EXPERIMENTAL MEASUREMENT

| Transmission Band | f_{sim} (GHz) | -3 dB BW (GHz) _{sim} | Ins. Loss (dB) _{sim} | f_{meas} (GHz) | -3 dB BW (GHz) _{meas} | Ins. Loss (dB) _{meas} |
|-------------------|-----------------|-------------------------------|-------------------------------|------------------|--------------------------------|--------------------------------|
| Main | 1.5 | 0.19 | 0.63 | 1.49 | 0.13 | 1.45 |
| LTB | 0.77 | 0.04 | 1.40 | 0.78 | 0.02 | 1.48 |
| UTB | 2.33 | 0.19 | 1.47 | 2.30 | 0.15 | 1.62 |

Comparisons between simulated and measured results are shown in Fig. 11. It is observed that the impedance level for the filter model decreases with frequency in both the EM simulation and the experimental results. The most important frequency ranges (LTB, Main, UTB) are precisely delimited by increases in the impedance levels, with the upper limits always being larger compared to the lower limits. Fig. 11(b) presents the Group Delay parameter, which expresses the delay of the response of a signal during its propagation along the filter structure. It is possible to observe maximum delays below 11 ns for the EM simulation and 15 ns for the signals results obtained via experimental measurement.

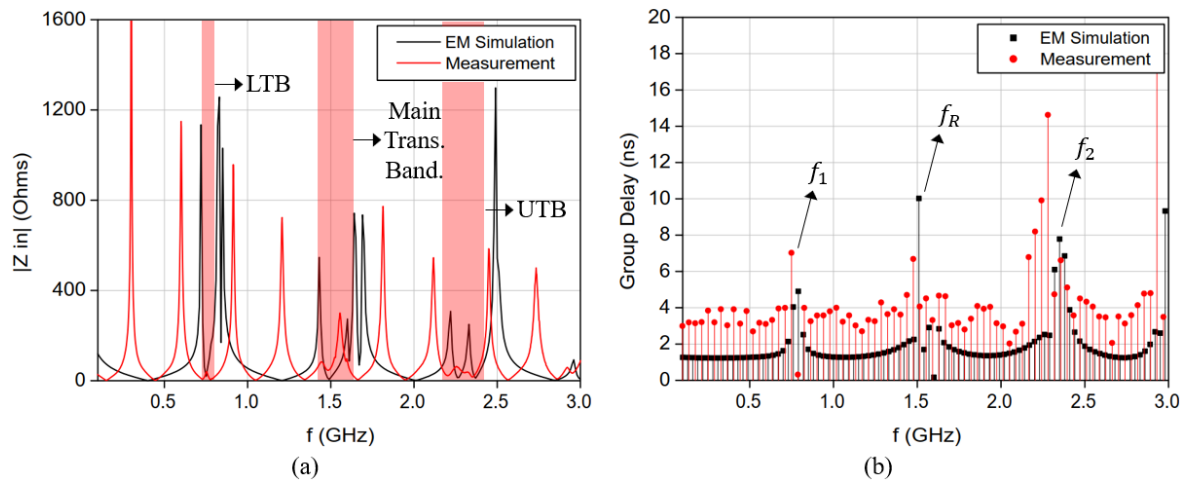


Fig. 11. (a) Comparison between input impedance Z_{in} as a function of frequency obtained by simulation and experimental measurement. (b) Group Delay.

Table II presents the comparison of the TBF modeled and proposed here with other recent works found in the literature, thus demonstrating their equivalence, from research focused on single-band structures to triple-band structures. The resonator geometries which the base works also have similar modeling processes.

TABLE II. COMPARISON BETWEEN PROPOSED TBF AND LITERATURE MODELS

| Model | f (GHz) | -3 dB BW(%) | N tz | Ins. Loss(dB) | Resonator |
|------------------|---------------------------|---------------------------|----------|---------------------------|--|
| [2] | 2.1 | 23.7 | 6 | 1.6 | Side-coupled Square Ring / Stub-loaded |
| [3] | 2 | 12 | 2 | 2.4 | Side-coupled Square Ring |
| [6] | 2.4 | 5 | 2 | 0.91 | Fractally Slotted Patch |
| [7] | 0.35 / 0.957 / 1.68 | 10.5 / 6.2 / 4.3 | 8 | 1.1 / 0.77 / 0.67 | Coupled Line / Stub-loaded |
| [13] | 2.1 / 2.62 | 1.76 / 1.527 | 3 | 0.81 / 1.13 | Coupled Feed Lines |
| [14] | 1.57 / 4.6 | 82.16 / 41.52 | 2 | 0.21 / 0.39 | Coupled Lines |
| [18] | 1.8 / 2.38 / 3.5 | 4 / 4.1 / 4 | 3 | 0.07 / 0.08 / 0.11 | Embedded Stub-loaded |
| [19] | 1.575 / 1.8 / 2.4 | 6.1 / 3.5 / 3.1 | 6 | 0.7 / 0.9 / 0.9 | Stub-loaded |
| [20] | 3.6 / 6 / 9 | 3 / 4.7 / 3.5 | 5 | 3.16 / 2.17 / 3.16 | Double CRLH |
| This work | 0.78 / 1.49 / 2.30 | 2.56 / 8.72 / 6.52 | 4 | 1.48 / 1.45 / 1.62 | Modified Side-coupled Square Ring |

V. CONCLUSION

A triple-bandpass filter based on a modification of the side-coupled square ring geometry had its design modeled and developed in this work. Expressions were obtained that describe both the admittance matrix and the filter geometry transformation. Analyzes based on the impedances described in the modeling were developed and described in order to obtain their respective influences on the frequency response of the model. A prototype was built and measurements were made in order to allow comparisons with the results obtained by means of EM simulation, which were very coherent and approximate to each other. Finally, comparisons between the proposed model and literature works have been presented, and the approach developed here is fully in line with the latest research involving microwave filter design.

ACKNOWLEDGMENT

This work was supported by CNPq under covenant 573939/2008-0 (INCT-CSF), CAPES and Federal University of Rio Grande do Norte (UFRN).

REFERENCES

- [1] Min, Xueliang & Zhang, Hou. Compact dual-band bandstop filter using folded resonator. *AEU-Inter. Journal of Electr. and Com.*, vol. 82, pp. 520-525, 2017.
- [2] K. Da Xu, Z. Luo, Y. Liu, Q. H. Liu, "High-selectivity single-ended and balanced bandpass filters using ring resonators and coupled lines loaded with multiple stubs," *AEU-Inter. Journal of Electr. and Com.*, vol. 96, pp. 193-198, 2018.
- [3] M. K. M. Salleh, G. Prigent, O. Pigaglio, R. Crampagne, "Quarter-wavelength side-coupled ring resonator for bandpass filters," *IEEE Trans. on Micro. Theory and Tech*, vol. 56, pp. 156-162, 2008.
- [4] C. -J. Chen, "A coupled-line coupling structure for the design of quasi-elliptic bandpass filters," *IEEE Trans. on Micro. Theory and Tech*, vol. 66, pp. 1921-1925, 2018.
- [5] R. T. Hamed, B. H. Hamed, "Compact multiple bandstop filter using integrated circuit of defected microstrip structure (DMS) and dual-mode resonator," *AEU-Inter. Journal of Electr. and Com.*, vol. 107, pp. 209-214, 2019.
- [6] S. Karthie, S. Salivahanan, "Fractally slotted patch resonator based compact dual-mode microstrip bandpass filter for Wireless LAN applications," *AEU-Inter. Journal of Electr. and Com.*, vol. 107, pp. 264-274, 2019.
- [7] V. K. Killamsetty, B. Mukherjee, "Compact triple band bandpass filters design using mixed coupled resonators," *AEU-Inter. Journal of Electr. and Com.*, vol. 107, pp. 49-56, 2019.
- [8] M. Orellana, J. Selga, P. Vélez, M. Sans, A. Rodríguez, J. Bonache, V. E. Boria, F. Martín, "Design of capacitively loaded coupled-line bandpass filters with compact size and spurious suppression," *IEEE Trans. on Micro. Theory and Tech*, vol. 65, pp. 1235-1248, 2017.
- [9] W. Feng, X. Gao, W. Che, Q. Xue, "Bandpass filter loaded with open stubs using dual-mode ring resonator," *IEEE Micro. and Wir. Comp. Let.*, vol. 25, pp. 295-297, 2015.
- [10] W. J. Feng, M. L. Hong, W. Q. Che, Q. Xue, "Dual-band microstrip bandstop filter with multiple transmission poles using coupled lines," *IEEE Micro. and Wir. Comp. Let.*, vol. 27, pp. 236-238, 2017.
- [11] X. Gao, W. Feng, W. Che, "High-selectivity wideband balanced filters using coupled lines with open/shorted stubs," *IEEE Micro. and Wir. Comp. Let.*, vol. 27, pp. 260-262, 2017.
- [12] M. Riaz, B. S. Virdee, P. Shukla, M. Onadim, "Quasi-elliptic ultra-wideband bandpass filter with super-wide stopband," *AEU-Inter. Journal of Electr. and Com.*, vol. 105, pp. 171-176, 2019.
- [13] A. Ghaderi, A. Golestanifar, F. Shama, "Microstrip bandpass filters using coupled feed lines for third and fourth generation communications," *AEU-Inter. Journal of Electr. and Com.*, vol. 86, pp. 195-201, 2018.
- [14] S. Y. Shriram, K. V. P. Kumar, S. S. Karthikeyan, "Compact dual-wideband bandpass filter for wireless applications," *AEU-Inter. Journal of Electr. and Com.*, vol. 95, pp. 69-72, 2018.
- [15] Y. Nemoto, K. Kobayashi, R. Sato, "Graph transformations of nonuniform coupled transmission line networks and their application," *IEEE Trans. on Micro. Theory and Tech*, vol. 33, pp. 1257-1263, 1985.
- [16] P. I. Richards, "Resistor-transmission-line circuits," *Proceed. of the IRE*, vol. 36, pp. 217-220, 1948.
- [17] H. Ozaki, J. Ishii, "Synthesis of a class of strip-line filters," *IRE Trans. on Circ. Theo.*, vol. 5, pp. 104-109, 1958.
- [18] F. Song, B. Wei, L. Zhu, Y. Feng, R. Wang, B. Cao, "A novel tri-band superconducting filter using embedded stub-loaded resonators," *IEEE Trans on Appl. Superc.*, vol. 26, pp. 1-9, 2016.
- [19] H. W. Wu, L. Y. Jian, Y. W. Chen, Y. K. Su, "New triple-passband bandpass filter using multipath stub loaded resonators," *IEEE Micro. and Wir. Comp. Let.*, vol. 26, pp. 186-188, 2016.
- [20] M. P. Mohan, A. Alphones, M. F. Karim, "Triple band filter based on double periodic CRLH resonator," *IEEE Micro. and Wir. Comp. Let.*, vol. 28, pp. 212-214, 2018.
- [21] K. Singh, S. Pal, D. Bhatnagar, "Notch Implementation in Planar Band Stop Filter using Step Impedance Resonator Approach," *Journal of Microw., Optoelect. and Electromag Appli. (JMoe)*, vol. 9, pp. 50-56, 2010.
- [22] C. P. Costa, A. G. D'Assunção, H. C. Nascimento, A. G. D'Assunção Junior, "Simulation and Design of a Bandpass Filter Based on Substrate Integrated E-Plane Waveguide," *Journal of Microw., Optoelect. and Electromag Appli. (JMoe)*, vol. 18, pp. 390-398, 2019.
- [23] A. O. Nwajana, A. Dainkeh, K. S. Yeo, "Substrate integrated waveguide (SIW) bandpass filter with novel microstrip-CPW-SIW input coupling," *Journal of Microw., Optoelect. and Electromag Appli. (JMoe)*, vol. 16, pp. 393-402, 2017.